Supporting Information

Functionalization of benzothiadiazole in magnesium-based metal-organic framework for C_2H_2/CO_2 separation

Haiyi Sun,[a] Yunlei Liu,[b] Meng Sun,[a] Fei Gao,[a] Xueying Feng,[a] Mingming Xu*[a,b] and Xiaokang Wang*[a]

[a]Shandong Key Laboratory of Intelligent Energy Materials, State Key Laboratory of Heavy Oil Processing, School of Materials Science and Engineering, China University of Petroleum (East China), Qingdao, Shandong 266580, China.
[b]Technology Inspection Center, Shengli Oilfield Company, SINOPEC, Dongying, Shandong, 257000, China.

*Corresponding author E-mail: xiaokangwang0625@163.com; xumingming.slyt@sinopec.com

Table of Contents

Experimental Procedures

Materials and instruments

All reagents were commercially available and used without further purification.

^{1}H NMR spectrum was obtained on an Inova 400 MHz spectrometer. Single crystal X-ray diffraction experiments were carried out on a SuperNova diffractometer equipped with mirror Cu-Kα radiation (λ = 1.54184 Å) and an Eos CCD detector. Powder X-ray diffraction (PXRD) was carried out on a Bruker D8-Focus Bragg-Brentano X-ray powder diffractometer equipped with a Cu sealed tube at 40 kV and 15 mA. Thermogravimetric analysis (TGA) was performed on a Mettler Toledo TGA/DSC1 instrument under a static N_2 atmosphere with a heating rate of 10°C/min at the range of 40-900°C. Gas sorption measurements were conducted on a Micrometritics ASAP 2020 surface area analyzer.

Synthesis of H_2BTDC ligand

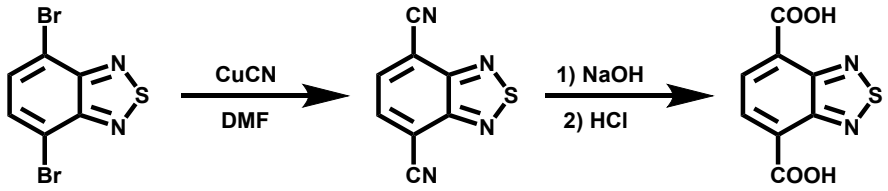

Scheme S1. Synthetic procedure for H_2BTDC.

A mixture of 4,7-dibromo-2,1,3-benzothiadiazole (11.9 mmol, 3.5 g), CuCN (24.1 mmol, 2.2 g), in 35 mL N,N'-dimethylformamide (DMF) was refluxed for 48 h under the N_2 atmosphere. The cooled mixture was poured into 2 M HCl (200 mL) and extracted with ethyl acetate (2 × 100 mL). The combined organic phase was washed with brine solution and then dried over anhydrous Na_2SO_4. The solvent was removed by rotary evaporation and the crude product was purified by column chromatography. After dissolved in 25% aqueous sodium hydroxide solution and refluxed for 24 h, the yellow solution was poured into 200 mL H_2O and acidified with concentrated HCl. The obtained reddish-brown precipitate was collected by filtration with a yield of 80%. ^{1}H NMR (400 MHz, DMSO-d_6) δ (ppm): 8.57 (d, 2H), 6.71 (d, 2H).

Synthesis of UPC-116

A mixture of H_2BTDC (4 mg) and $Mg(NO_3)_2 \cdot 6H_2O$ (20 mg) in 3 mL N,N'-dimethylformamide (DMF)/dioxane/H_2O (v/v/v = 5/2/1) was placed into a glass vial (10 mL) and heated at 100°C for 48 h. The vial was then cooled to room temperature at a rate of 5°C/h. The obtained brownish red block crystals (3.6 mg, 70% yield based on H_2BTDC) were filtered, washed with DMF and dried in air.

Single-crystal X-ray diffraction

The as-synthesized crystals were taken from the mother liquid without further treatment, transferred to oil and mounted on to a loop for single crystal X-ray data collection. The data were collected on an Agilent Technologies SuperNova diffractometer equipped with graphite monochromatic Cu Kα radiation (λ = 1.54184 Å). With the help of Olex2, the structure was solved with the Superflip structure solution program using charge flipping and refined with the ShelXL refinement package using least squares minimization. The structure was treated anisotropically, whereas the hydrogen atoms were placed in calculated ideal positions and refined as riding on their respective nonhydrogen atoms. PLATON and SQUEEZE were used to calculate the diffraction contribution of the solvent molecules and thereby produced a set of partly solvent-free diffraction intensities.

Gas sorption measurements

The activated samples were prepared by immersing the as-synthesized MOFs in chromatography-grade methanol and dichloromethane for solvent exchange, followed by activation under vacuum for 8 h at 373 K. Gas adsorption experiments containing C_2H_2 and CO_2 at 273 and 298 K, and N_2 at 77 K were performed by using ASAP-2020 surface area analyzer. The Brunauer-Emmett-Teller (BET) specific surface area and the pore size distribution were calculated based on the N_2 adsorption isotherm at 77 K. Liquid nitrogen bath was used to stabilize the temperature at 77 K, whereas other test temperatures were maintained via a circulating water bath.

Breakthrough experiments

Breakthrough experiments were carried out on BSD-MAB multi-component adsorption breakthrough curve analyzer. The activated samples were packed in a quartz tube and further flushed with He at 373 K for 10 h with a flow rate of 15 mL/min. During the experiments at 298 K, the equimolar C_2H_2/CO_2 mixture was used at a flow rate of 2 mL/min, and the outlet gas was monitored by Hiden HPR-20EGA mass spectrometer. The captured gas during the breakthrough experiment can be recovered by desorption process at 298 K with He at a flow rate of 10 mL/min.

Computational methods

Isosteric heat of adsorption

A Virial equation comprising the temperature-independent parameters a_i and b_j was employed to calculate the enthalpies of adsorption for C_2H_2 and CO_2, which were measured at 273 and 298 K.

$$\ln P = \ln N + \frac{1}{T}\sum_{i}^{m} a_i N_i + \sum_{j}^{n} b_j N_j$$

$$Q_{st} = -R\sum_{i=0}^{m} a_i N_i$$

Here, P is the pressure expressed in mmHg, N is the amount absorbed in mmol/g, T is the temperature in K, a_i and b_j are virial coefficients, and m, n represent the number of coefficients required to adequately describe the isotherms (herein, m =5 and n = 2). Q_{st} is the coverage-dependent isosteric heat of adsorption and R is the universal gas constant.

Selectivity based on ideal adsorbed solution theory

Before estimating the selectivity for binary gas mixture, the single-component gas adsorption isotherms were first fitted to dual-site Langmuir-Freundlich (DSLF) model:

$$q = q_{A,sat}\frac{b_A p^{n_1}}{1 + b_A p^{n_1}} + q_{B,sat}\frac{b_B p^{n_2}}{1 + b_B p^{n_2}}$$

where q is the amount of adsorbed gas (mmol/g), p is the bulk gas phase pressure (kPa), q_{sat} is the saturation amount (mmol/g), b is the Langmuir-Freundlich parameter (kPa^{-1}), and n is the Langmuir-Freundlich exponent (dimensionless) for two adsorption sites A and B indicating the presence of weak and strong adsorption sites. b_A and b_B are both temperature-dependent.

$$b_A = b_{A0}\exp\left(\frac{E_A}{RT}\right);\ b_B = b_{B0}\exp\left(\frac{E_B}{RT}\right)$$

The adsorption selectivity S_{ads} was calculated by ideal adsorbed solution theory:

$$S_{ads} = \frac{q_1/q_2}{p_1/p_2}$$

where q_1 and q_2 are the molar loadings in the adsorbed phase in equilibrium with the bulk gas phase, p_1 and p_2 are partial pressure.

Grand canonical Monte Carlo simulations

Grand canonical Monte Carlo (GCMC) simulations were carried out using the Sorption module of Materials Studio package. The Locate and Metropolis methods were used to predict the possible binding sites of C_2H_2 and CO_2 onto the framework. During the simulation, the C_2H_2 and CO_2 molecules including the frameworks were considered as rigid bodies. The optimal adsorption sites were simulated under 298 K and 100 kPa by the fixed loading task and Metropolis method. The atomic partial charges of the host MOF skeleton and all gas molecules were obtained from QEq method. The equilibration steps and the production steps were set to 5.0×10^6 and 1.0×10^7, respectively. The gas-skeleton interaction and the gas-gas interaction were characterized by the standard universal force field (UFF). The cut-off radius used for the Lennard-Jones interactions is 15.5 Å and the long-range electrostatic interactions were considered by the Ewald summation method.

Density functional theory calculations

Density functional theory (DFT) calculations were performed using Dmol3 module embedded in the Materials Studio software. Since it is a vast task to do the DFT calculations using a whole MOF unit cell, we used fragmented cluster models cleaved from unit cells representing the actual situations as high as possible, and the cleaved bonds at cluster boundaries were saturated by protons. The generalized gradient approximation (GGA) with the Perdewe Burkee Ernzerh of (PBE) exchange-correlation functional was employed for the spin-unrestricted DFT calculations. The electronic wave functions were expanded by the double numerical plus polarization (DNP) basis set. The van der Waals correction was considered by Grimme to precisely describe the adsorption/penetration of gas molecules on/through the g-GYN and g-GYH membranes. The convergence criterion was 1×10^5 Ha for energies, 2×10^3 Ha/Å for forces, and 5×10^3 Å for atomic displacements. The global cutoff radius was set as 6.0 Å. In all the DFT calculations, all the atoms were allowed to fully relax. The

adsorption energy (ΔE_{ads}) is expressed by

$$\Delta E_{ads} = E_{ads+fram} - E_{fram} - E_{ads}$$

where $E_{ads+fram}$, E_{fram}, and E_{ads} are the total energy of the adsorbate-framework adsorption system, adsorbent framework, and adsorbate molecule, respectively.

Figures S1-S12

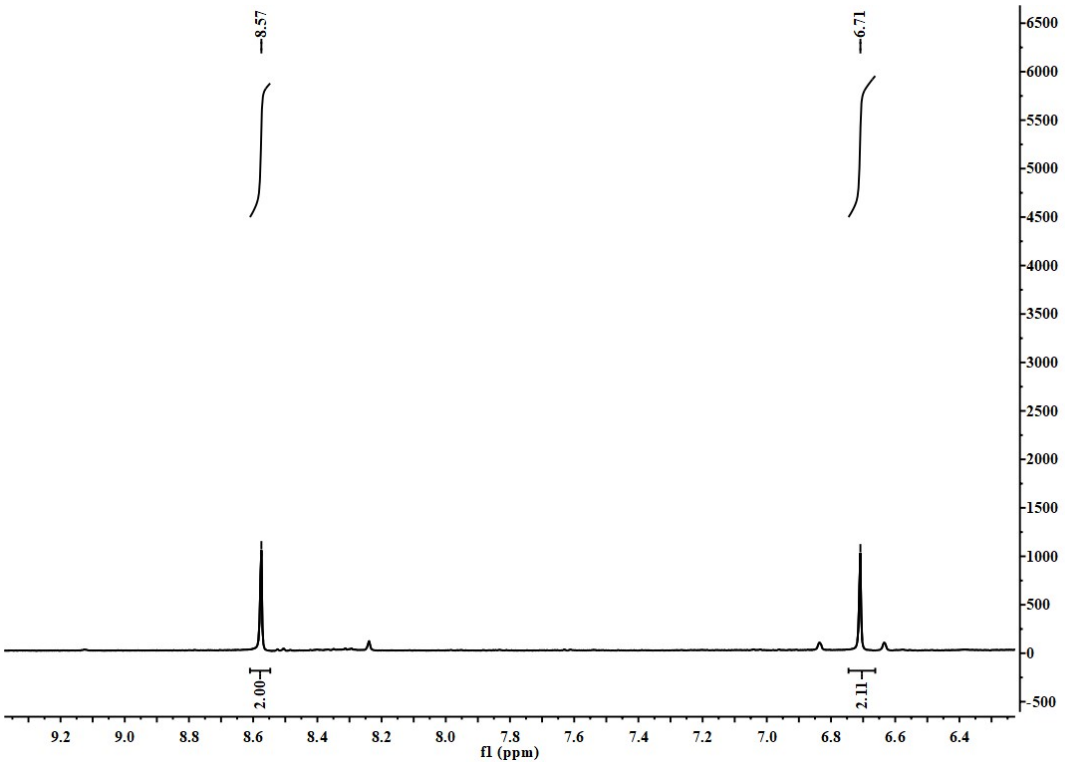

Fig. S1 ^{1}H NMR spectrum of H_2BTDC.

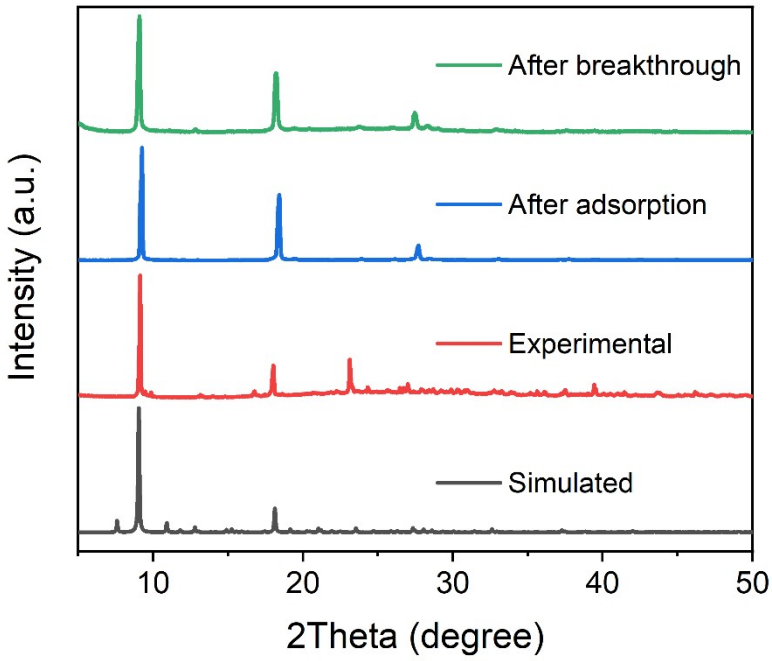

Fig. S2 PXRD patterns of UPC-116.

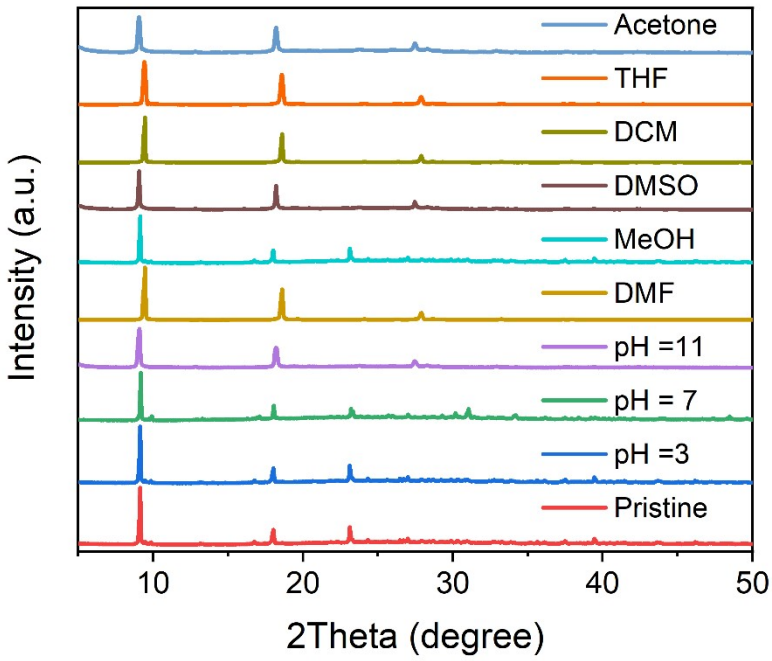

Fig. S3 PXRD patterns of UPC-116 after treatment in different solutions for 24 h.

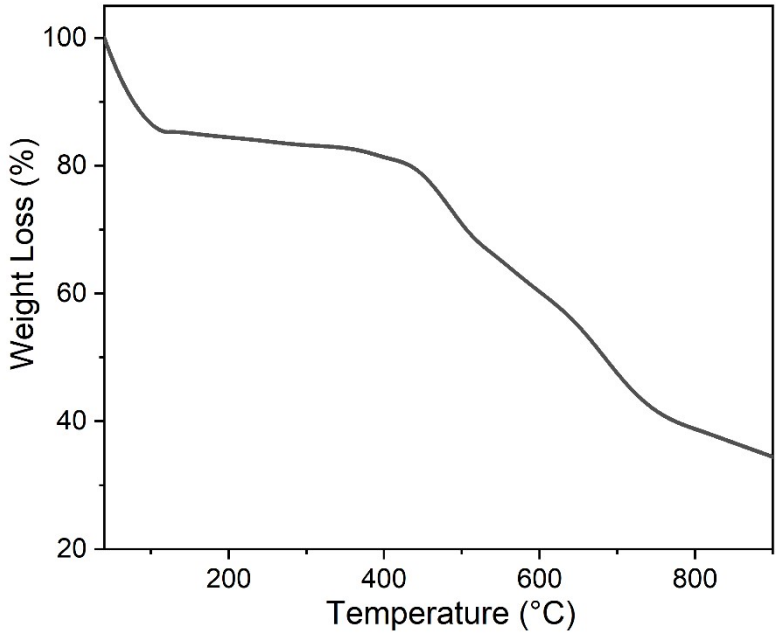

Fig. S4 TGA curve of UPC-116.

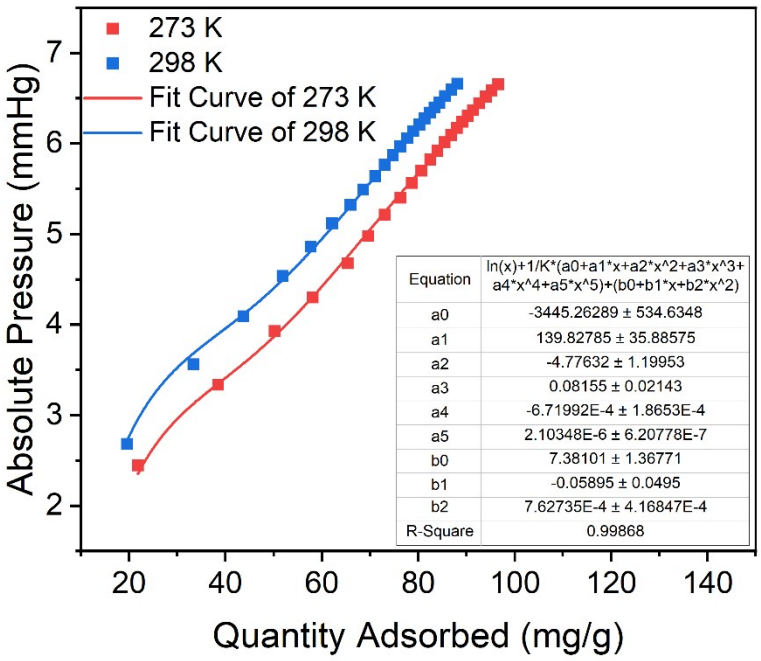

Fig. S5 Virial fitting of C_2H_2 for UPC-116.

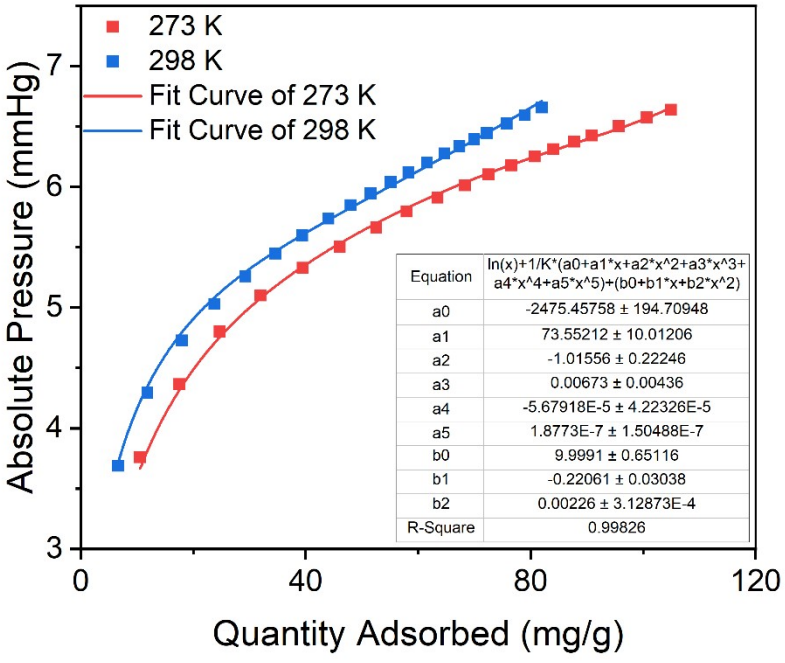

Fig. S6 Virial fitting of CO_2 for UPC-116.

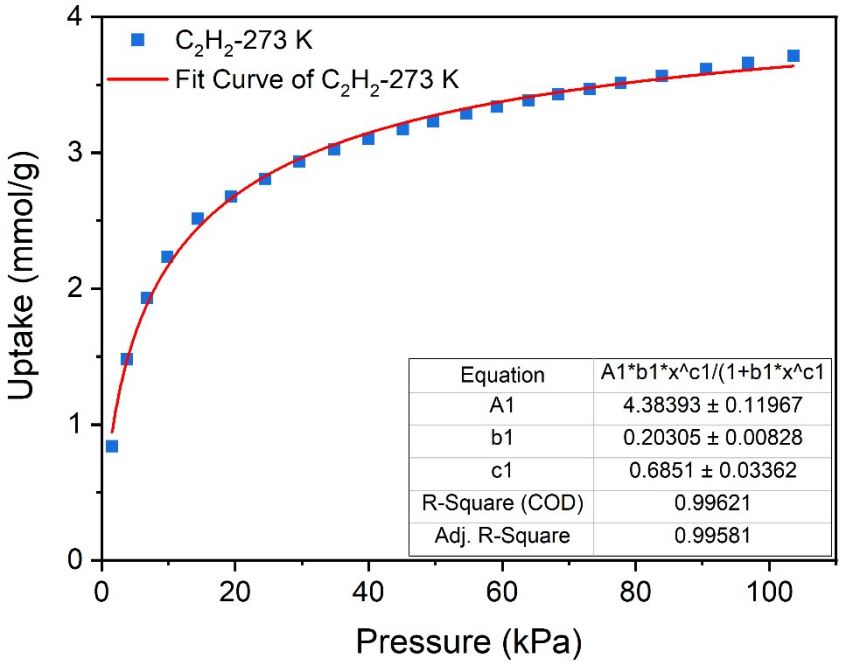

Fig. S7 Langmuir-Freundlich fitting of C_2H_2 for UPC-116 at 273 K.

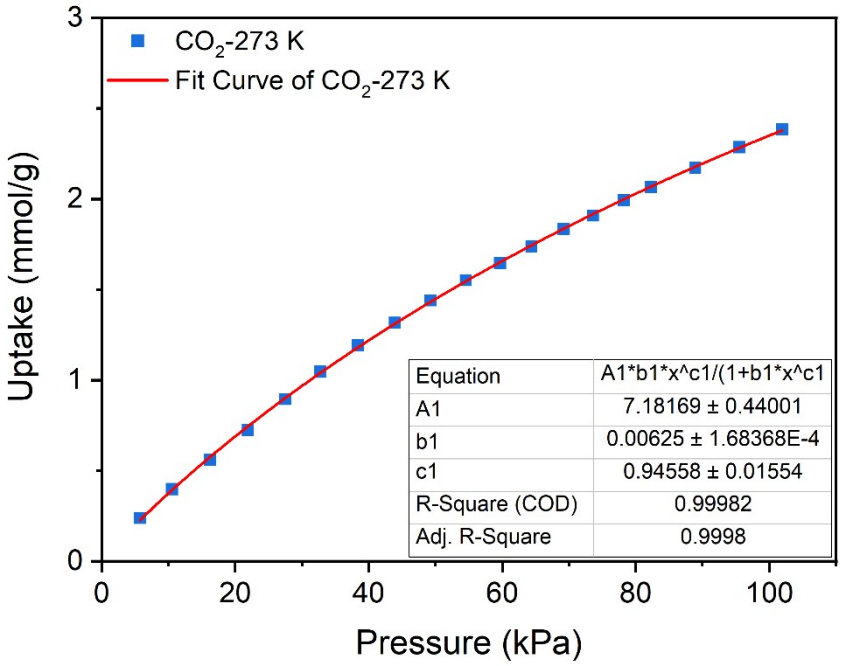

Fig. S8 Langmuir-Freundlich fitting of CO_2 for UPC-116 at 273 K.

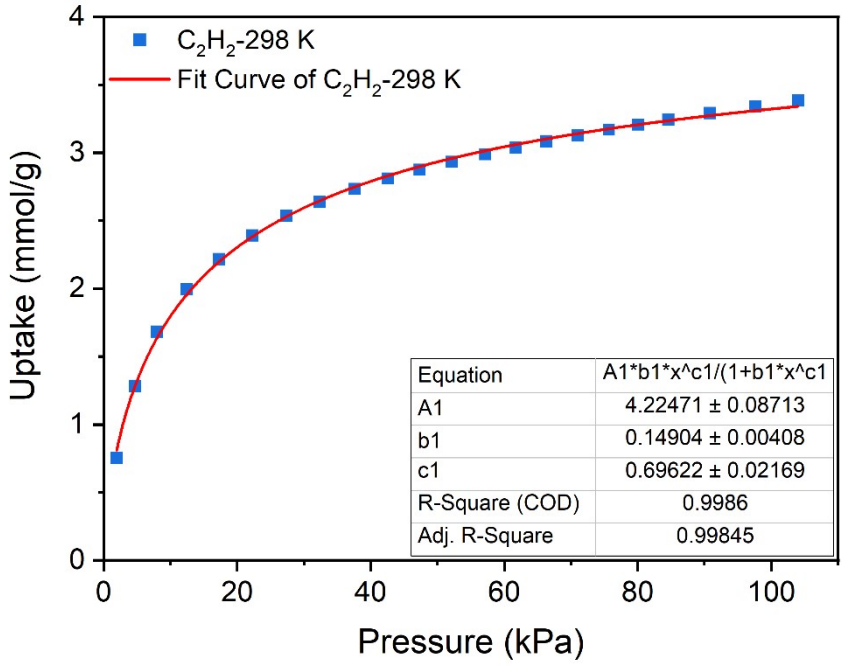

Fig. S9 Langmuir-Freundlich fitting of C_2H_2 for UPC-116 at 298 K.

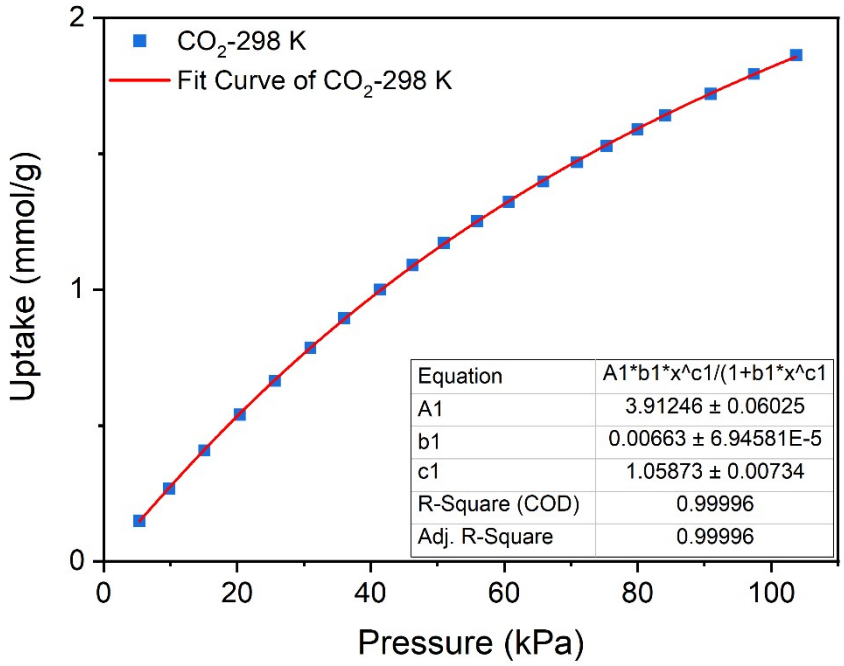

Fig. S10 Langmuir-Freundlich fitting of CO_2 for UPC-116 at 298 K.

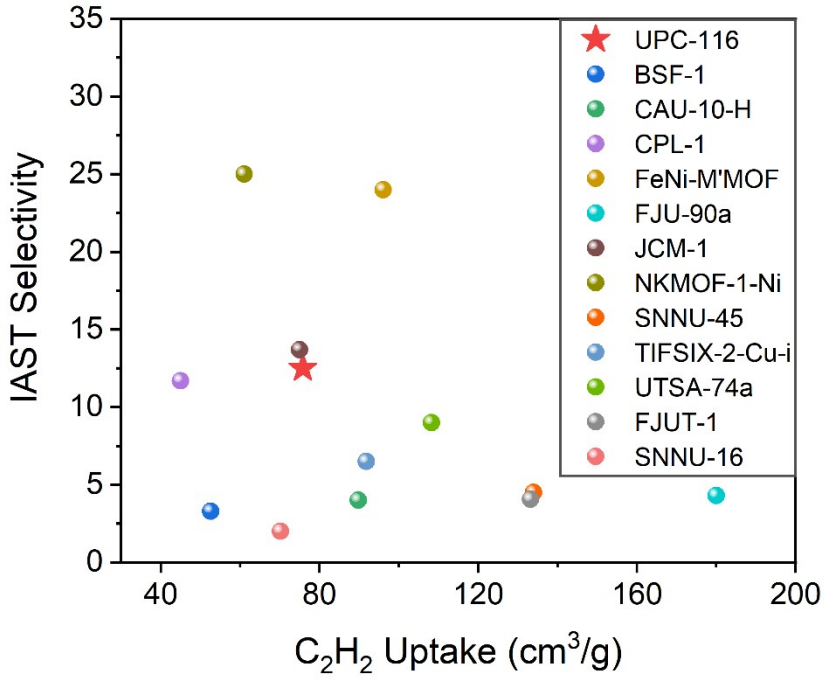

Fig. S11 Comparison of C_2H_2 uptake and IAST selectivity of equimolar C_2H_2/CO_2 with reported MOFs at 298 K.

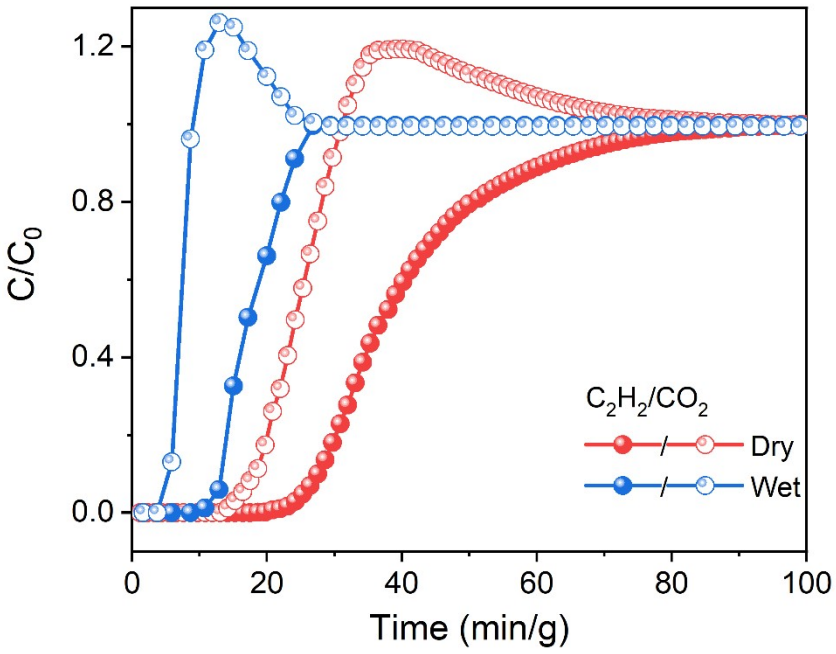

Fig. S12 Breakthrough curves of equimolar C_2H_2/CO_2 mixture (2 mL/min) on UPC-116 under dry and humid condition at 298 K and 1 bar.

Tables S1-S4

Table S1. Crystal data of UPC-116.

Compound	UPC-116
CCDC	2505745
Formula	$C_{23.5}H_{21.5}Mg_2N_{6.5}O_{10.5}S_2$
Formula weight	675.71
Temperature/K	293(2)
Crystal system	tetragonal
Space group	$P4_12_12$
a/Å	19.58922(16)
b/Å	19.58922(16)
c/Å	14.53473(18)
α/°	90
β/°	90
γ/°	90
Volume/Å^3	5577.52(11)
Z	8
ρ g/cm^3	1.609
μ/mm^{-1}	2.812
F(000)	2740.0
2θ range for data collection	7.574 to 141.346
Index ranges	$-23 \leq h \leq 16$ $-23 \leq k \leq 17$ $-17 \leq l \leq 15$
Reflections collected	11861
R_{int}	0.0265
Data/restraints/parameters	5201/0/290
Goodness-of-fit on F^2	1.058
Final R indexes [I>=2σ (I)]	$R_1 = 0.0343$ $wR_2 = 0.0925$
Final R indexes [all data]	$R_1 = 0.0369$ $wR_2 = 0.0948$
Largest diff. peak/hole /eÅ^{-3}	0.22/-0.39

Table S2. Comparison of separation performance in MOFs at 298 K.

Materials	C_2H_2 uptake (cm^3/g)	C_2H_2 Q_{st} (kJ/mol)	IAST selectivity	Ref.
UPC-116	83.20	28.64	12.27	This work
BSF-1	52.6	31	3.3	[1]
CAU-10-H	89.8	27.4	4.0	[2]
CPL-1	45.0	45.5	11.7	[3]
FeNi-M'MOF	96.1	27	24	[4]
FJU-90a	180	25.1	4.3	[5]
JCM-1	75	36.9	13.7	[6]
JNU-1	–	13	3.6	[7]
$Ni(4\text{-}DPDS)_2CrO_4$	67.0	75.4	67.7	[8]
NKMOF-1-Ni	61.0	60.3	25	[9]
SNNU-45	134	39.9	4.5	[10]
TIFSIX-2-Cu-i	91.8	46.3	6.5	[11]
UTSA-300a	68.9	57.6	743	[12]
UTSA-74a	108.2	31	9	[13]
ZJU-74	85.7	45	36.5	[14]
FJUT-1	133.2	43.75	4.06	[15]
JXNU-5	55.9	32.9	–	[16]
M'MOF-2a	–	37.7	1.89	[17]
Ni(dpip)	83.6	41.7	2	[18]
SNNU-16	70.2	52.6	2.0	[19]

Table S3 Raw gas adsorption data of UPC-116 at 273 K.

C_2H_2 adsorption		C_2H_2 desorption		CO_2 adsorption		CO_2 desorption	
Pressure (kPa)	Uptake (cm^3/g)	Pressure (kPa)	Uptake (cm^3/g)	Pressure (kPa)	Uptake (cm^3/g)	Pressure (kPa)	Uptake (cm^3/g)
1.54216	18.82015	103.60772	83.20696	4.31114	7.32737	105.13564	75.66018
3.75572	33.11618	97.17458	82.10697	8.28455	13.08894	98.91816	73.99207
6.78308	43.23492	91.10969	81.07097	12.80728	19.58502	93.08317	72.22423
9.83282	50.033	85.0509	80.01785	17.3829	25.62023	87.09763	70.20565
14.35148	56.32429	78.71542	78.8633	22.08264	31.01051	81.21788	68.05719
19.39504	59.9676	72.50201	77.64016	26.91461	35.82664	75.61685	65.88748
24.46505	62.90519	66.64057	76.41604	31.78931	40.20492	70.09925	63.55404
29.54931	65.73102	60.83203	75.13183	36.59077	44.18573	64.38836	60.98878
34.8126	67.76146	55.20659	73.77152	41.27626	47.54135	58.89517	58.25433
39.93551	69.48729	49.41636	72.25925	46.1123	50.77843	53.47318	55.3085
45.10929	71.07189	43.74616	70.6544	50.55569	53.5814	48.24244	52.24992
49.61777	72.31478	38.17769	68.89511	54.818	56.00991	43.05849	48.87762
54.57385	73.61293	32.6906	66.94285	59.50145	58.42366	37.85827	45.22942
59.22069	74.77764	25.99501	63.75554	64.01197	60.68813	32.78622	41.2252
63.94687	75.81651	19.18955	59.81916	68.82767	62.86131	26.36733	35.53881
68.40653	76.80908	13.20197	54.72385	73.59861	64.87986	20.69713	29.82514
73.0676	77.75493	7.95496	45.84712	77.86906	66.68112	15.68001	24.02416
77.73682	78.68318			81.93199	68.15639	10.92942	17.60097
83.88513	79.81483			86.23906	69.70354	6.58166	10.64305
90.4973	80.96637			92.62541	71.83596		
96.82668	82.04749			98.73506	73.76029		
103.60772	83.20696			105.13564	75.66018		

Table S4 Raw gas adsorption data of UPC-116 at 298 K.

C_2H_2 adsorption		C_2H_2 desorption		CO_2 adsorption		CO_2 desorption	
Pressure (kPa)	Uptake (cm^3/g)	Pressure (kPa)	Uptake (cm^3/g)	Pressure (kPa)	Uptake (cm^3/g)	Pressure (kPa)	Uptake (cm^3/g)
1.94907	16.85483	104.00242	75.87957	5.33654	3.35678	103.683	41.71629
4.70177	28.7564	97.4818	74.81773	9.76975	6.0089	97.30072	40.24385
7.97327	37.68877	91.13411	73.79612	15.07169	9.14503	91.1809	38.68402
12.4492	44.66964	84.82914	72.71523	20.36144	12.08816	85.12008	37.04022
17.25676	49.66094	78.64218	71.573	25.61252	14.87988	79.30746	35.41642
22.27795	53.55463	72.58339	70.39487	30.95516	17.60754	73.42161	33.66911
27.36831	56.78478	66.64464	69.19557	35.98245	20.03649	67.53576	31.8491
32.33456	59.07492	60.66926	67.79238	41.36171	22.405	61.73739	29.98955
37.54089	61.22111	54.69593	66.34131	46.24862	24.41315	56.06515	28.10195
42.58445	62.95751	49.01963	64.86469	50.90562	26.24419	50.49872	26.08421
47.28825	64.39871	43.33112	63.18628	55.9146	28.05154	45.04215	23.91738
52.09988	65.6937	37.74841	61.29256	60.6652	29.64209	39.48588	21.57906
57.12107	66.94629	32.16163	58.99518	65.82269	31.31347	34.03135	19.09381
61.71907	68.04272	24.54847	54.99541	70.89271	32.89875	27.63483	15.91236
66.25605	69.11735	17.82643	50.10269	75.34423	34.25478	21.05521	12.46641
70.9395	70.06011	12.08502	44.10165	79.94427	35.60307	15.26294	9.3095
75.6372	71.01674	6.90108	34.76131	84.05806	36.76171	9.89182	6.08111
80.05617	71.83474			90.94286	38.53778		
84.55041	72.66725			97.39431	40.18722		
90.73737	73.73227			103.683	41.71629		
97.57945	74.83345						
104.00242	75.87957						

References

(1) Zhang, Y.; Yang, L.; Wang, L.; Duttwyler, S.; Xing, H. A Microporous Metal-Organic Framework Supramolecularly Assembled from a Cu^{II} Dodecaborate Cluster Complex for Selective Gas Separation. *Angew. Chem. Int. Ed.* **2019**, *58* (24), 8145−8150. DOI: 10.1002/anie.201903600.

(2) Pei, J.; Wen, H. M.; Gu, X. W.; Qian, Q. L.; Yang, Y.; Cui, Y.; Li, B.; Chen, B.; Qian, G. Dense Packing of Acetylene in a Stable and Low-Cost Metal-Organic Framework for Efficient C_2H_2/CO_2 Separation. *Angew. Chem. Int. Ed.* **2021**, *60* (47), 25068−25074. DOI: 10.1002/anie.202110820.

(3) Yang, L.; Yan, L.; Wang, Y.; Liu, Z.; He, J.; Fu, Q.; Liu, D.; Gu, X.; Dai, P.; Li, L.; Zhao, X. Adsorption Site Selective Occupation Strategy within a Metal–Organic Framework for Highly Efficient Sieving Acetylene from Carbon Dioxide. *Angew. Chem. Int. Ed.* **2021**, *60* (9), 4570−4574. DOI: 10.1002/anie.202013965.

(4) Gao, J.; Qian, X.; Lin, R. B.; Krishna, R.; Wu, H.; Zhou, W.; Chen, B. Mixed Metal–Organic Framework with Multiple Binding Sites for Efficient C_2H_2/CO_2 Separation. *Angew. Chem. Int. Ed.* **2020**, *59* (11), 4396−4400. DOI: 10.1002/anie.202000323.

(5) Ye, Y.; Ma, Z.; Lin, R.-B.; Krishna, R.; Zhou, W.; Lin, Q.; Zhang, Z.; Xiang, S.; Chen, B. Pore Space Partition within a Metal–Organic Framework for Highly Efficient C_2H_2/CO_2 Separation. *J. Am. Chem. Soc.* **2019**, *141* (9), 4130−4136. DOI: 10.1021/jacs.9b00232.

(6) Lee, J.; Chuah, C. Y.; Kim, J.; Kim, Y.; Ko, N.; Seo, Y.; Kim, K.; Bae, T. H.; Lee, E. Separation of Acetylene from Carbon Dioxide and Ethylene by a Water-Stable Microporous Metal–Organic Framework with Aligned Imidazolium Groups inside the Channels. *Angew. Chem. Int. Ed.* **2018**, *57* (26), 7869−7873. DOI: 10.1002/anie.201804442.

(7) Zeng, H.; Xie, M.; Huang, Y. L.; Zhao, Y.; Xie, X. J.; Bai, J. P.; Wan, M. Y.; Krishna, R.; Lu, W.; Li, D. Induced Fit of C_2H_2 in a Flexible MOF Through Cooperative Action of Open Metal Sites. *Angew. Chem. Int. Ed.* **2019**, *58* (25), 8515−8519. DOI: 10.1002/anie.201904160.

(8) Zheng, F.; Chen, R.; Ding, Z.; Liu, Y.; Zhang, Z.; Yang, Q.; Yang, Y.; Ren, Q.; Bao, Z. Interlayer Symmetry Control in Flexible-Robust Layered Metal–Organic Frameworks for Highly Efficient C_2H_2/CO_2 Separation. *J. Am. Chem. Soc.* **2023**, *145* (36), 19903−19911. DOI: 10.1021/jacs.3c06138.

(9) Peng, Y. L.; Pham, T.; Li, P.; Wang, T.; Chen, Y.; Chen, K. J.; Forrest, K. A.; Space, B.; Cheng, P.; Zaworotko, M. J.; Zhang, Z. Robust Ultramicroporous Metal–Organic Frameworks with Benchmark Affinity for Acetylene. *Angew. Chem. Int. Ed.* **2018**, *57* (34), 10971−10975. DOI: 10.1002/anie.201806732.

(10) Li, Y. P.; Wang, Y.; Xue, Y. Y.; Li, H. P.; Zhai, Q. G.; Li, S. N.; Jiang, Y. C.; Hu, M. C.; Bu, X. Ultramicroporous Building Units as a Path to Bi-microporous Metal–Organic Frameworks with High Acetylene Storage and Separation Performance. *Angew. Chem. Int. Ed.* **2019**, *58* (38), 13590−13595. DOI: 10.1002/anie.201908378.

(11) Chen, K.-J.; Scott, Hayley S.; Madden, David G.; Pham, T.; Kumar, A.; Bajpai, A.; Lusi, M.; Forrest, Katherine A.; Space, B.; Perry, John J.; Zaworotko, Michael J. Benchmark C_2H_2/CO_2 and CO_2/C_2H_2 Separation by Two Closely Related Hybrid Ultramicroporous Materials. *Chem* **2016**, *1* (5), 753−765. DOI: 10.1016/j.chempr.2016.10.009.

(12) Lin, R.-B.; Li, L.; Wu, H.; Arman, H.; Li, B.; Lin, R.-G.; Zhou, W.; Chen, B. Optimized Separation of Acetylene from Carbon Dioxide and Ethylene in a Microporous Material. *J. Am. Chem. Soc.* **2017**, *139* (23), 8022−8028. DOI: 10.1021/jacs.7b03850.

(13) Luo, F.; Yan, C.; Dang, L.; Krishna, R.; Zhou, W.; Wu, H.; Dong, X.; Han, Y.; Hu, T.-L.; O'Keeffe, M.; Wang, L.; Luo, M.; Lin, R.-B.; Chen, B. UTSA-74: A MOF-74 Isomer with Two Accessible Binding

Sites per Metal Center for Highly Selective Gas Separation. *J. Am. Chem. Soc.* **2016**, *138* (17), 5678−5684. DOI: 10.1021/jacs.6b02030.
(14) Pei, J.; Shao, K.; Wang, J. X.; Wen, H. M.; Yang, Y.; Cui, Y.; Krishna, R.; Li, B.; Qian, G. A Chemically Stable Hofmann-Type Metal−Organic Framework with Sandwich-Like Binding Sites for Benchmark Acetylene Capture. *Adv. Mater.* **2020**, *32* (24), 1908275. DOI: 10.1002/adma.201908275.
(15) Zhang, L.; Xiao, T.; Zeng, X.; You, J.; He, Z.; Chen, C.-X.; Wang, Q.; Nafady, A.; Al-Enizi, A. M.; Ma, S. Isoreticular Contraction of Cage-like Metal–Organic Frameworks with Optimized Pore Space for Enhanced C_2H_2/CO_2 and C_2H_2/C_2H_4 Separations. *J. Am. Chem. Soc.* **2024**, *146* (11), 7341−7351. DOI: 10.1021/jacs.3c12032.
(16) Liu, R.; Liu, Q.-Y.; Krishna, R.; Wang, W.; He, C.-T.; Wang, Y.-L. Water-Stable Europium 1,3,6,8-Tetrakis(4-carboxylphenyl)pyrene Framework for Efficient C_2H_2/CO_2 Separation. *Inorg. Chem.* **2019**, *58* (8), 5089−5095. DOI: 10.1021/acs.inorgchem.9b00169.
(17) Xiang, S.-C.; Zhang, Z.; Zhao, C.-G.; Hong, K.; Zhao, X.; Ding, D.-R.; Xie, M.-H.; Wu, C.-D.; Das, M. C.; Gill, R.; Thomas, K. M.; Chen, B. Rationally Tuned Micropores within Enantiopure Metal-Organic Frameworks for Highly Selective Separation of Acetylene and Ethylene. *Nat. Commun.* **2011**, *2*, 204. DOI: 10.1038/ncomms1206.
(18) Li, Y.-Z.; Wang, G.-D.; Ma, L.-N.; Hou, L.; Wang, Y.-Y.; Zhu, Z. Multiple Functions of Gas Separation and Vapor Adsorption in a New MOF with Open Tubular Channels. *ACS Appl. Mater. Interfaces* **2021**, *13* (3), 4102–4109. DOI: 10.1021/acsami.0c21554.
(19) Li, H.-P.; Dou, Z.-D.; Wang, Y.; Xue, Y. Y.; Li, Y. P.; Hu, M.-C.; Li, S.-N.; Jiang, Y.-C.; Zhai, Q.-G. Tuning the Pore Surface of an Ultramicroporous Framework for Enhanced Methane and Acetylene Purification Performance. *Inorg. Chem.* **2020**, *59* (22), 16725–16736. DOI: 10.1021/acs.inorgchem.0c02713.